Ecosystems (2004) 7: 545–562
DOI: 10.1007/s10021-004-0144-5

ECOSYSTEMS

Spectral and Structural Measures of Northwest Forest Vegetation at Leaf to Landscape Scales

Dar A. Roberts,[1]* Susan L. Ustin,[2] Segun Ogunjemiyo,[1] Jonathan Greenberg,[2] Solomon Z. Dobrowski,[2] Jiquan Chen,[3] and Thomas M. Hinckley[4]

[1]*Department of Geography, EH3611, University of California, Santa Barbara, California, 93106, USA;* [2]*Department of Air, Land, and Water Resources, University of California, Davis, California, 95616, USA;* [3]*Department of Earth, Ecological, and Environmental Sciences, University of Toledo, Toledo, Ohio 43606, USA;* [4]*College of Forest Resources, University of Washington, Seattle, Washington 98195, USA*

Abstract

We report a multiscale study in the Wind River Valley in southwestern Washington, where we quantified leaf to stand scale variation in spectral reflectance for dominant species. Four remotely sensed structural measures, the normalized difference vegetation index (NDVI), cover fractions from spectral mixture analysis (SMA), equivalent water thickness (EWT), and albedo were investigated using Airborne Visible Infrared Imaging Spectrometer (AVIRIS) data. Discrimination of plant species varied with wavelength and scale, with deciduous species showing greater separability than conifers. Contrary to expectations, plant species were most distinct at the branch scale and least distinct at the stand scale. At the stand scale, broadleaf and conifer species were spectrally distinct, as were most conifer age classes. Intermediate separability occurred at the leaf scale. Reflectance decreased from leaf to stand scales except in the broadleaf species, which peaked in near-infrared reflectance at the branch scale. Important biochemical signatures became more pronounced spectrally progressing from leaf to stand scales. Recent regenerated clear-cuts (less than 10 years old) had the highest albedo and non-photosynthetic vegetation (NPV). After 50 years, the stands showed significant decreases in albedo, NPV, and EWT and increases in shade. Albedo was lowest in old-growth forests. Peak EWT, a proxy measure for leaf area index (LAI), was observed in 11- to 30-year-old stands. When compared to LAI, EWT and NDVI showed exponentially decreasing, but distinctly different, relationships with increasing LAI. This difference is biologically important: at 95% of the maximum predicted NDVI and EWT, LAI was 5.17 and 9.08, respectively. Although these results confirm the stand structural variation expected with forest succession, remote-sensing images also provide a spatial context and establish a basis to evaluate variance within and between age classes. Landscape heterogeneity can thus be characterized over large areas—a critical and important step in scaling fluxes from stand-based towers to larger scales.

Key words: remote sensing; canopy architecture; leaf area index; albedo; conifer forests; broadleaf deciduous forests; spatial scale; AVIRIS; imaging spectroscopy.

Introduction

The conifer forests of the Pacific Northwest are economically and biologically important ecosystems that have undergone extensive alteration over the past 120 years. It is difficult to predict the scale-dependent consequences of climate change and changing atmospheric chemistry in such extensively disturbed forested landscapes. To meet this challenge, an integrated research program was initiated at several sites within the Gifford Pinchot

Received 15 February 2002; accepted 1 August 2003; published online 20 May 2004.
*Corresponding author; e-mail: dar@geog.ucsb.edu

National Forest to quantify organism- to ecosystem-level fluxes of carbon and water (Suchanek and others 2004). Studies at these sites and elsewhere have demonstrated that species and age differences in forest stands affect fluxes of carbon and water. Although remote sensing provides a basis for scaling fluxes to the region, we have no means of interpreting these data in terms of stand characteristics that would lead to a more detailed understanding of composition and structure and therefore enable modeling at this larger scale. Specifically, this study was designed to provide a more regional context to point-measurements made at a pair of flux sites located in the Wind River old-growth forest in the Gifford Pinchot National Forest. Remote sensing is a critical component in scaling forest function and structure because it provides a regional context for detailed, but localized, site measurements (Running 1994; Potter and others 1993; Sellers and others 1996).

The Pacific Northwest has a rich history of remote-sensing research, primarily centered over the Oregon Transect, extending from coastal forests to the east side of the Cascade range (Peterson and Waring 1994). Remote sensing has been used to estimate leaf area index (LAI) (Peterson and others 1987; Spanner and others 1994; Law and Waring 1994a; Gong and others 1995), canopy chemistry (Johnson and others 1994), the spatial distribution of land-cover types (Cohen and others 1995), stand height (Lefsky and others 1999; Means and others 1999), primary productivity (Law and Waring 1994b), and stand structure (Cohen and others 1990; Cohen and Spies 1992; Sabol and others 2002). These studies have demonstrated the scaling utility of remote sensing.

Our primary objective was to learn how the spectral signal of different plant species changes across multiple scales (from leaves to canopies to landscapes), thus extending the work of Goward and others (1994). Understanding these spectral changes will enable us to address the ability of remote sensing to detect and distinguish biophysical features across these scales. A secondary objective was to evaluate how representative stands surrounding the two flux towers were of other equal-aged stands from the surrounding landscape. Specifically, our study provides a regional context for the two intensive flux sites. We chose two approaches for data analysis to reflect how spectral features change across scales as different properties are incorporated into the measurement (for example, anatomical differences at the leaf level, branch structure and LAI at the canopy level, and tree gaps and age or size distribution at the landscape level). At leaf and branch scales, our primary focus was on comparing spectra from plant species. At the stand or landscape scale, the analysis shifted toward a comparison of a variety of spectral indices that are sensitive to stand structure.

Methods

Two scale-dependent approaches were used to address our objectives. At the leaf scale, chemical properties of the leaf (for example, chlorophyll content) control wavelength specific absorbance patterns, whereas morphological features (for instance, leaf thickness) control the scattering process (Gates and others 1965; Woolley 1971). At this level, we measured both spectral reflectance and transmission. At the branch scale, the spatial arrangement of canopy elements (for example, leaves, shoots, reproductive structures, bark, epiphytes, and so on) and their light-absorbing and scattering properties dominate (Asner 1998). Reflected light is then a mixture of the strong absorptive properties of leaves in the visible and scattering of near-infrared (NIR) light by all branch and canopy elements. At the stand/landscape scale, there is again an interplay between biochemical absorption and physical scattering. Typically, at this scale reflectance data are a composite of how absorption and scattering are mixed at the level of the pixel. Because each pixel is the sum of often very different elements (for example, a broadleaf tree in the sun, a conifer in the shade, and a patch of bare soil), its analysis is very different from the relatively simple comparisons that can be done at the leaf or branch scales. Although the quantity of green foliage or LAI tends to dominate the reflectance from any pixel, differences in canopy structure and member architecture can significantly alter the reflectance (Asner 1998). As in other scaling exercises, reflectance of a pixel at the landscape level cannot be directly calculated as the integrated sum of the reflectances of all of the different elements found within that pixel. Our techniques were thus designed to analyze and compare the following three scales: leaf (resolution, 2×2 cm), branch (30×30 cm), and stand/landscape (AVIRIS, 20×20 m).

Study Site

The study site comprised a 12×36 km area defined by an airborne visible infrared imaging spectrometer (AVIRIS) flight line (Figure 1); it included the old-growth site at the Wind River Canopy Crane Research Facility (WRCCRF) (Shaw and others 2004), the surrounding T. T. Munger Research Nat-

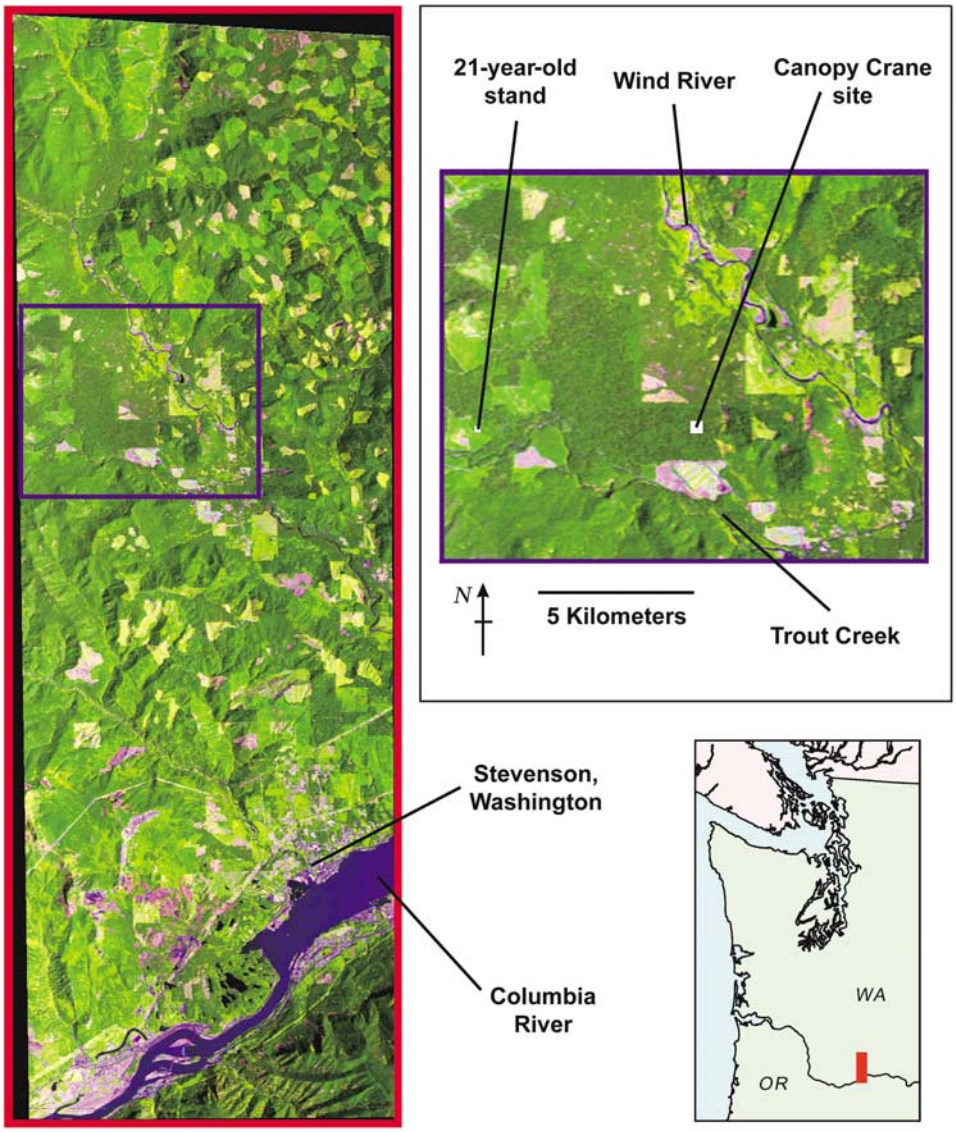

Figure 1. The July 1998 AVIRIS flightline and the location of the old-growth and "20"-year-old flux tower sites. The larger white square in the inset to the right marks the location of the Wind River Canopy Crane Research Facility (WRCCRF). The smaller white square in the inset marks the location of the tower in the 21-year-old stand. The "20"-year flux tower is located on the eastern edge of the 21-year-old stand. See Chen and others (2004) for a description of the flux measurements.

ural Area, and the "20"-year-old stand flux site (Chen and others 2004). Because the stand was 21 years old when the image was acquired, it is called "the 21-year-old stand" throughout the text. Elevation ranges from less than 30 m in the south to over 1,000 m in the north. A complete description of the physical site characteristics is provided by Shaw and others (2004).

The area is mostly forested and includes a diversity of age classes of Douglas-fir (*Pseudotsuga menziesii*); a mixture of 100-, 160-, and 500-year old-growth Douglas-fir/western hemlock (*Tsuga heterophylla*), recently regenerated to fairly old clear-cuts (0–100-year classes); and riparian zones. At least eight conifer species, four broadleaf tree species, and 16 deciduous and evergreen shrubs and forbs are dominants or codominants at the largest spatial resolution used in this study. Species studied in detail here included four conifers (*Pinus monticola* [PIMO]), *Pseudotsuga menziesii* [PSME], *Tsuga heterophylla* [TSHE], and *Thuja plicata* [THPL]), five broadleaf trees *(Populus trichocarpa* [POTR], *Acer macrophyllum* [ACMA], *Acer circinatum* [ACCI], *Alnus rubra* [ALRU], and *Cornus nuttallii* [CONU]), and four epiphytes *(Platismatia glauca* [PLGL], *Lobaria oregana* [LOOR], *Isothecium stoloniferum* [ISST], and an assemblage of Alectoroid lichens [ALLI]).

Spectral Data and Image Analysis

Leaf scale. Either one sunlit leaf (broadleaf) or a sunlit branchlet (conifer) with current foliage from each of two to four sapling-sized trees was collected from the upper canopy on the south side of each

tree in May 1988. After harvesting, leaves or foliated branchlets were immediately stored in a cooler during transport to the lab. Hemispherical reflectance and transmittance were measured between 200 and 2,350 nm at 2-nm intervals from both leaf surfaces using a Beckman DK2a (Beckman Instruments, Fullerton, CA, USA) with an integrating sphere and standardized to reflectance using a halon calibration panel. Because an individual needle did not cover the sample port, needles were aligned on a slide mount to minimize gaps and overlaps before measurement. In addition to leaf spectra, spectra of nonvascular epiphytes, litter, and bark were acquired with a Cary-5E (Varian, Sunnyvale, CA, USA) with a Labsphere integrating sphere (Labsphere, North Sutton, NH, USA).

Branch scale. Branch-scale spectra, between 350 and 2,500 nm at 2-nm sampling intervals, were measured in the field using an ASD-FR spectrometer (Analytical Spectral Devices, Boulder, CO, USA) between 1 and 9 September 1999. Spectra were standardized to reflectance using Spectralon (Labsphere, North Sutton, NH, USA). Spectra were collected at two heights, between 0.5 and 1 m above the target branch, using a 22° field of view (19–38 cm radius) and at heights of up to 60 m or more using a 8° foreoptic (radius, 8 m). All spectra were collected within 2.5 h of solar noon.

To capture intraspecies variability in reflectance, multiple measurements were made of different branches within an individual and on different individuals of each species. Our general approach was to develop a list of common plant species in the area, then identify locations close to roads where plants could be accessed from the ground or a 3-m ladder. A total of seven sites were identified, primarily consisting of recently regenerated clear-cuts and forest edges. The sites ranged in elevation from 180 to 750 m and were located within a 7-km radius of the WRCCRF. Once target species were identified, spectra were acquired of both branches on individuals and branches from different individuals of the same species. The number of measurements made per plant varied depending on the variability of each target and access. For small-stature shrubs and grasses, most spectra are from individual plants. For taller trees and shrubs, multiple measurements were typically required to account for variation at a scale larger than the field of view of the instrument. In total, over 40 individual trees were measured, including 12 PSME, seven TSHE, six ACMA, and two THPL. The total number of spectra for each species varied between five and 32. To avoid the effects of illumination extremes on spectra, extremely bright targets (representing a single leaf) and dark targets (shadows) were not included in the calculation of the mean or variance.

Landscape scale. Canopy-scale and stand-scale spectra were derived from AVIRIS data acquired on 17 July, 1998 at 17:43 universal time coordinate (UTC) (zenith [θ], 39.5°; azimuth [ϕ], 63.9°). AVIRIS collects 224 spectral bands between 370 and 2,500 nm at a sampling interval of approximately 10 nm and a resolution of approximately 20 $\times$ 20 m (Green and others 1998). Because most spectra at 20-m resolution are mixed, either consisting of multiple plant species or multiple plants, our analysis at these scales focused on plant species only and on locations where a single species was known to dominate a stand. Within the AVIRIS flight line, this limited our analysis to several age classes of PSME, two age classes of TSHE, and a few stands of ALRU.

AVIRIS image analysis. Although the information presented in Figure 1 tends to be translated by the human eye/brain as a picture of the landscape where clear-cuts of various ages, topographic features, rivers, roads, settlements, and so on, can be easily seen, imbedded within each 20 $\times$ 20 m pixel forming this scene is 224 individual wavelengths of data from which information about stand composition and structure can be calculated. In addition, it is scenes such as this one that form the foundation for scaling stand data to the landscape level, both via an understanding of the range of a given attribute, its pattern and its variation, but also via an ability to aggregate pixels (that is, stands) of similar attributes.

Several remotely sensed measures (or attributes) derived from AVIRIS images that are sensitive to stand structure were analyzed, including equivalent water thickness (EWT), normalized difference vegetation index (NDVI), spectral mixture analysis (SMA), and albedo. AVIRIS data were processed to apparent surface reflectance using the model of Green and others (1993) and Roberts and others (1997). This approach compensates for changes in water vapor associated with topography and variable air masses. Liquid water produces a strong absorption that is approximately 40 nm longer than the wavelengths of water vapor absorption (Green and others 1991). This spectral difference enables simultaneous retrieval of column water vapor and liquid water. EWT (in μm) is calculated by fitting measured reflectance between 865 and 1,085 nm to the equivalent transmittance spectrum of a slab of water (calculated using a Beer-Lambert model) and varying path length until a minimum difference is achieved.

NDVI is the most widely used index in remote sensing, particularly as an estimate of LAI, the fraction of absorbed photosynthetically active radiation (PAR), and percent cover (Tucker 1979; Sellers 1985; Gamon and others 1994). NDVI was calculated as the ratio of (NIR−red)/(NIR+red) by convolving AVIRIS reflectance spectra to the equivalent Landsat Thematic Mapper (TM) bands for TM4 (NIR) and TM3 (red).

Although NDVI is most commonly used to estimate LAI, a recent paper suggested that EWT may be more appropriate (Roberts and others 1998a). To evaluate the relationship among LAI, NDVI, and EWT, we compared LAI estimated from these two remotely sensed variables to LAI measured in the field (described later).

Subpixel fractions of canopy components were estimated using SMA. SMA linearly decomposes a mixed spectrum into more fundamental spectral components weighted by their abundance (Smith and others 1990; Adams and others 1993). Typical forest components include soil, nonphotosynthetic vegetation (NPV) (litter, bark, branches), green vegetation (GV) (foliage), and shade (plus shadows). Branch-scale spectra and field spectra of soils and NPV measured in the area were used as endmembers for the AVIRIS analysis. A four-endmember model consisting of a single set of GV (PSME branch), NPV (PSME bark), soil, and shade was used. Shade was set to 0% reflectance across all wavelengths (photometric shade). The best set of endmembers was selected following techniques described by Roberts and others (1998b) designed to constrain endmember selection to produce fractions that are consistent with field estimates.

Albedo was calculated as the sum of the product of modeled surface irradiance and AVIRIS apparent surface reflectance between 370 and 2,500 nm for each pixel. This calculation differs from what is properly termed "planetary albedo", which integrates reflected flux across all view angles and wavelengths for a specific incidence angle by incorporating a function that describes how surface reflectance varies as a function of view azimuth and zenith (the bidirectional reflectance distribution function). In the case of a diffuse (Lambertian) surface, "directional" albedo will be the same as the true albedo of the surface. Surface irradiance was modeled using Modtran 3.5 radiative transfer code (Berk and others 1989) parameterized to match the elevation, date, and time of acquisition and latitude and longitude of the AVIRIS overpass. Modeled irradiance was convolved to AVIRIS wavelengths, then subsetted to remove regions of strong atmospheric absorption. Once subsetted, modeled irradiance was multiplied by the same wavelength subset of apparent surface reflectance and summed across all wavelengths for each pixel imaged.

Data Analysis

Stand Age. All image products were georeferenced to a digital elevation model derived from US Geological Survey (USGS) topographic quad maps using nearest-neighbor resampling. Stand age was determined from a digital stand age map obtained from the US Forest Service (USFS) (http://www.fs-.fed.us/gpnf/gis/gpveg1998). Ages were combined into seven classes—less than 5 years, 6–10, 11–30, 31–50, 51–100, 101–200, and old growth (more than 200 years). After coregistering the AVIRIS products and the USFS age map, areal statistics for albedo, GV, NPV, NDVI, shade, and EWT were calculated for these age classes of PSME stands.

Leaf and branch data. To determine the statistical significance of spectral differences between species at leaf and branch scales, we employed a two-sample *t*-test for each wavelength measured. We tested the null hypothesis that the means of two spectra were not significantly different at an α of at least 0.05.

Leaf area index: field data collection and analysis. Using the analyzed EWT image as a guide, a large number of sites covering a wide range of EWT values were identified and then visited. From this initial group, 39 sites were selected for further study. Differential GPS positions were determined using a PDOP mask of 8 or less and range-finding binoculars (horizontal accuracy, ±2 m) when necessary. LAI was measured using a LiCor LAI-2000 (LiCor., Lincoln, NE, USA) with a 90° view angle restrictor oriented either south or west. The LAI-2000 was held at eye height (around 1.5 m) and kept at least 50 cm from any leaves. At each site, 10 measurements were taken at 1-m intervals along a transect oriented perpendicular to the direction of the LAI-2000. To minimize direct light incident on the lens, all measurements were taken before or shortly after sunrise and after sunset. A second LAI-2000 was placed in an open field facing the same cardinal direction as the LAI-2000 used under the canopy. Both instruments were calibrated together before each crepuscular data collection.

To determine overstory species cover and understory LAI, two 20-m transects at ±15° of the cardinal direction were established at each site. Every 2 m along each transect, a densiometer was used to determine the overstory species cover and a weighted line was lowered slowly into the understory from eye height (around 1.5 m). For each leaf the line touched, the angle of that leaf to the near-

est 45° was recorded (Thomas and Winner 2000). All moss intercepts were recorded.

Uncorrected LAI was calculated using the LAI-2000 software, masking the fourth and fifth lens angles to minimize topographic influences. Methods and parameters published in Frazer and others (2000) were used to correct the LAI values, which tend to be underestimated in conifer forests. For each site, we calculated the percent cover by species based on the densiometer results. The corrected overstory LAI (LAI_{over}) for each site was calculated as:

$$LAI_{over} = LAI_{uncor} \sum_{i=1}^{n} s c_i r_i \quad (1)$$

where LAI_{uncor} is the uncorrected LAI calculated from the LAI-2000 software, s is the shape factor ($s = 1.18$), i is the species index number, n is the maximum number of species found in all sites, c_i is the fractional cover of species i, and r_i is the mean needle–shoot area ratio published by Frazer and others (2000). For the three species that did not have published needle–shoot area ratios, we used published values from taxonomically and structurally similar species. Calibration factors (mean needle–shoot area ratio) included 2.352 (*Abies procera* and generic *Abies*), 2.178 (PSME), 1.385 (*Taxus brevifolia* and TSHE), and 1.014 (THPL). A shape factor of 1.0 was used for all nonconifers.

The understory LAI (LAI_{under}) for each site was estimated as a ratio of the number of leaves intercepted by the line (lth) to the number of times the line was dropped (dth). Finally, total LAI for a given site (LAI_{total}) was the sum of over and understory LAI for that site.

Leaf area index: estimation from AVIRIS (NDVI and EWT). Regions of interest (ROI) were created for each of the 39 LAI sampling sites using four pixels roughly matching the LAI-2000 coverage, or a single pixel for sites with no vegetation. The mean EWT and NDVI for these ROI (EWT_{site}, $NDVI_{site}$) was calculated. Several pixels with no living plant matter were chosen and assigned an LAI of 0.000001. Nonlinear regression models of the following form were used for analysis using the SAS PROC NLIN procedure (SAS Institute, Cary, NC, USA):

$$EWT_{site} = (b - be^{-aLAI_{total}}) + c \quad (2)$$

$$NDVI_{site} = (v - ve^{-uLAI_{total}}) + w \quad (3)$$

These models assume an exponential decay in which the rate of increase in NDVI or EWT decreases as the number of leaves in the canopy or LAI increases. Parameters b and v can be considered the maximum value of either index once the relationship has reached an asymptote, parameters a or u function as a dampening or extinction coefficients, and c or w equal the fitted intercept at 0 LAI. We compared the LAI value at 95% of the estimated EWT and NDVI asymptote (b and v, respectively).

Results

Spectral Properties of Materials at Different Scales

Leaf scale reflectance. Hemispherical leaf reflectance and transmittance spectra were measured for three dominant broadleaf and three dominant conifer tree species (Figure 2). At the leaf scale, within-species variance was low, especially in the visible range. Strong chlorophyll absorption, at 450 and 680 nm, and slightly weaker liquid water bands, centered at 1,400 and 1,900, represent the major absorption features (Gates and others 1965; Woolley 1971). A general trend of decreasing transmittance and reflectance beyond 1,350 nm is due to the presence of a very strong liquid water absorption feature centered at 2,700 nm, just outside the range of the instrument. Photon scattering dominates the NIR. Weak liquid water absorption features are also evident at 980 and 1,200 nm.

A comparison between the broadleaf and conifer species showed marked differences in leaf spectra. Conifers had slightly lower visible reflectance, higher NIR (830 nm) reflectance, and lower shortwave infrared (SWIR, 1,650–2,500 nm) reflectance than broadleaf species. In conifers, the spectral contrast between NIR and SWIR was particularly diagnostic; the contrast between these two wavelengths was greater than that found in any broadleaf species. Liquid water absorptions at 980 and 1,200 nm were also deeper than in broadleaf species.

To assess whether spectral differences between tree species were statistically significant, we employed a two-sample t-test and compared pairs of mean spectra (Table 1). Based on this analysis, we conclude that spectral separability varies considerably between species pairs. In general, species within the same taxonomic category were the least distinct, but they could still be distinguished based on some portion of the spectrum. For example, within broadleaf tree species, the proportion of bands that were statistically distinct ranged from 34.1% to 75.6%, suggesting that all three species could be easily distinguished. In contrast for conifers, the proportion of bands that were statistically distinct was far lower, ranging from a low of 13.6%

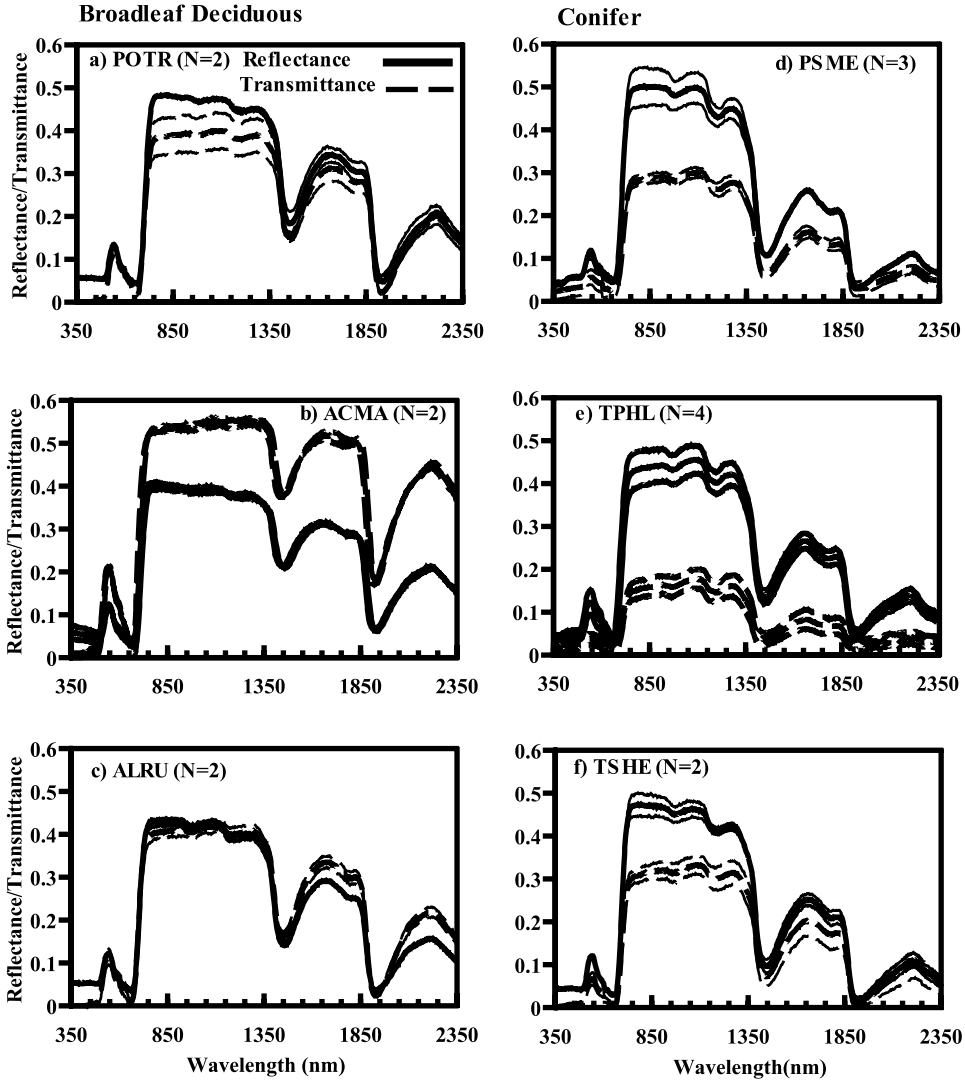

Figure 2. Leaf-level hemispherical reflectance and transmittance spectra of three broadleaf and three conifer dominants. Reflectance is plotted as a solid line; transmittance, as a dashed line. Plots show the mean ± SD. The number of spectra taken is shown in parentheses. Species names follow the codes in the text. POTR, *Populus trichocarpa*; ACMA, *Acer macrophyllum*; ALRU, *Alnus rubra*; PSME, *Pseudotsuga menziesii*; THPL, *Thuja plicata*; TSHE, *Tsuga heterophylla*.

for the PSME-TSHE pair to a high of 26.3% for PSME and THPL.

In almost all cases, differences between conifers and broadleaf trees were greater than within a taxonomic category. For example, PSME was spectrally distinct from the broadleaf tree species in 54% to 83% of the wavelengths. TSHE showed even greater separability, ranging from 76.3% to 88.2%. The one exception was ALRU, which was more similar to THPL than it was to the other broadleaf spectra.

To determine which wavelengths are critical for separating plant species, we plotted the *t*-statistics for each species pair and for all 1,050 spectral bands examined (data not shown). Here we compared pairs of broadleaf species, conifers, and conifers paired with a broadleaf tree species. For *t*-values, statistically significant differences were defined for α less than or equal to 0.05. Of the broadleaf comparisons, the ALRU-ACMA pair was most distinct in the SWIR (more than 1,350 nm), still significantly distinct in the NIR, but not in the visible portion of the spectrum. The ALRU-POTR pair, in contrast, was less distinct throughout most of the SWIR, but it was more distinct in the NIR and visible wavelengths. The ACMA-POTR pair was spectrally distinct primarily in the NIR (700–1,350 nm).

In contrast to the broadleaf species, conifers were only distinct within very specific spectral regions. For example, the PSME-TSHE pair was only spectrally distinct in the green (550 nm) and red (680 nm) absorption regions of chlorophyll, the red-edge reflectance region (700–730 nm), and a region centered around 1,900 nm. The THPL-TSHE pair was only distinct in the SWIR, in regions centered at 1,400 and 1,900 nm (that is, strong liquid water bands). The PSME-THPL pair was spectrally distinct throughout much of the SWIR, but not in the NIR

Table 1. Spectral Separability between Tree Species at Leaf and Branch Scales

	Leaf Scale					
Species	**PSME**	**THPL**	**TSHE**	**ALRU**	**ACMA**	**POTR**
PSME	*	26.27	13.59	83.02	80.42	53.65
THPL	82.74	*	22.98	23.98	47.65	46.15
TSHE	28.11	89.81	*	88.21	85.71	76.32
ALRU	81.6	49.15	74.43	*	71.33	75.62
ACMA	99.81	56.13	99.81	89.06	*	34.07
POTR	99.81	67.45	98.96	99.25	13.77	*
			Branch Scale			

PSME, Pseudotsuga menzlesii; THPL, Thuja plicata; TSHE, Tsuga heterophylla; ALRU, Alnus rubra; ACMA, Acer macrophyllum; POTR, Populus trichocarpa
Columns and rows report the percentage of total bands that were significantly different ($\alpha = 0.05$). Values above the diagonal represent paired leaf-scale comparisons; those below the diagonal represent, paired branch-scale comparisons. A higher percentage indicates more statistically different wavelengths.

or visible portions of the spectrum. Most wavelengths were statistically significant when comparing a broadleaf and conifer pair; however, the most critical spectral region was the SWIR, although the NIR was spectrally distinct for the TSHE-ACMA pair. Select portions of the visible spectrum were important for all comparisons between conifers and broadleaf tree species.

In contrast to reflectance data, greater spectral differences in transmittance were found among species (Figure 2). Within broadleaf species, high SWIR transmittance was measured for ACMA, with peak transmittances nearly equal to the NIR transmittance. Lowest transmittance was observed in POTR. Within conifers, the highest transmittance was measured in TSHE, followed by PSME. THPL had very low transmittance, equal to or less than 20% in the NIR. When broadleaf and conifer spectra were compared, transmittance was two to three times lower in conifers across the entire spectrum, although the differences were not statistically significant due to high variance and small sample sizes. Transmittance differences between species are important in that they tend to magnify leaf level differences at the branch and then at stand or landscape scales due to multiple scattering. Lower transmittance in conifers suggests that conifers tend to absorb more incident radiation than broadleaf deciduous stands, independent of canopy structure.

Branch Scale Reflectance Mean (± 1 SD) branch-scale spectra ($n = 6$–26) were calculated for five broadleaf and five conifer dominants (Figure 3). Branch-level spectra contrasted with leaf level and demonstrated increased within-species spectral variability at most wavelengths, although the difference was only significant in the NIR ($\alpha = 0.01$). However, spectral differences between species also increased, enhancing spectral separation. For example, POTR and ACMA, which had similar NIR and SWIR reflectance, could be separated based on higher visible light reflectance in ACMA. ACCI and ALRU, which had lower reflectance than POTR and ACMA at all wavelengths, were also distinct based on their visible reflectance. CONU was distinct from all species by having relatively high visible reflectance, low NIR reflectance, and very low SWIR reflectance for a broadleaf species. Spectral differences between conifers were more subtle: PIMO, PSME, and TSHE showed only minor (less than 5%) spectral differences at all wavelengths. ABAM was distinguished by lower reflectance at all wavelengths. THPL had the highest reflectance across all wavelengths, with visible, NIR, and SWIR reflectance equal to or exceeding some broadleaf species.

Statistical analysis demonstrated enhanced spectral separability at the branch versus the leaf scale (Table 1). For example, PSME and TSHE, which were distinct in only 13.6% of the 1,050 sample wavelengths at the leaf scale, were distinct in 28.1% of the wavelengths at the branch scale. In most paired comparisons, more than 80% of the wavelengths were significantly different (that is, PSME versus ACMA). The one exception was ACMA and POTR, which decreased from 34.1% separation at the leaf scale to 13.8% at the branch scale. Because these two species represented the extremes in reflectance and transmittance at the leaf scale (ACMA had the highest transmittance and lowest reflectance; POTR had the highest reflectance and lowest transmittance), their branch-scale comparison suggests that multiple light scattering within a canopy tends to balance out extreme differences between transmittance and reflectance of leaves.

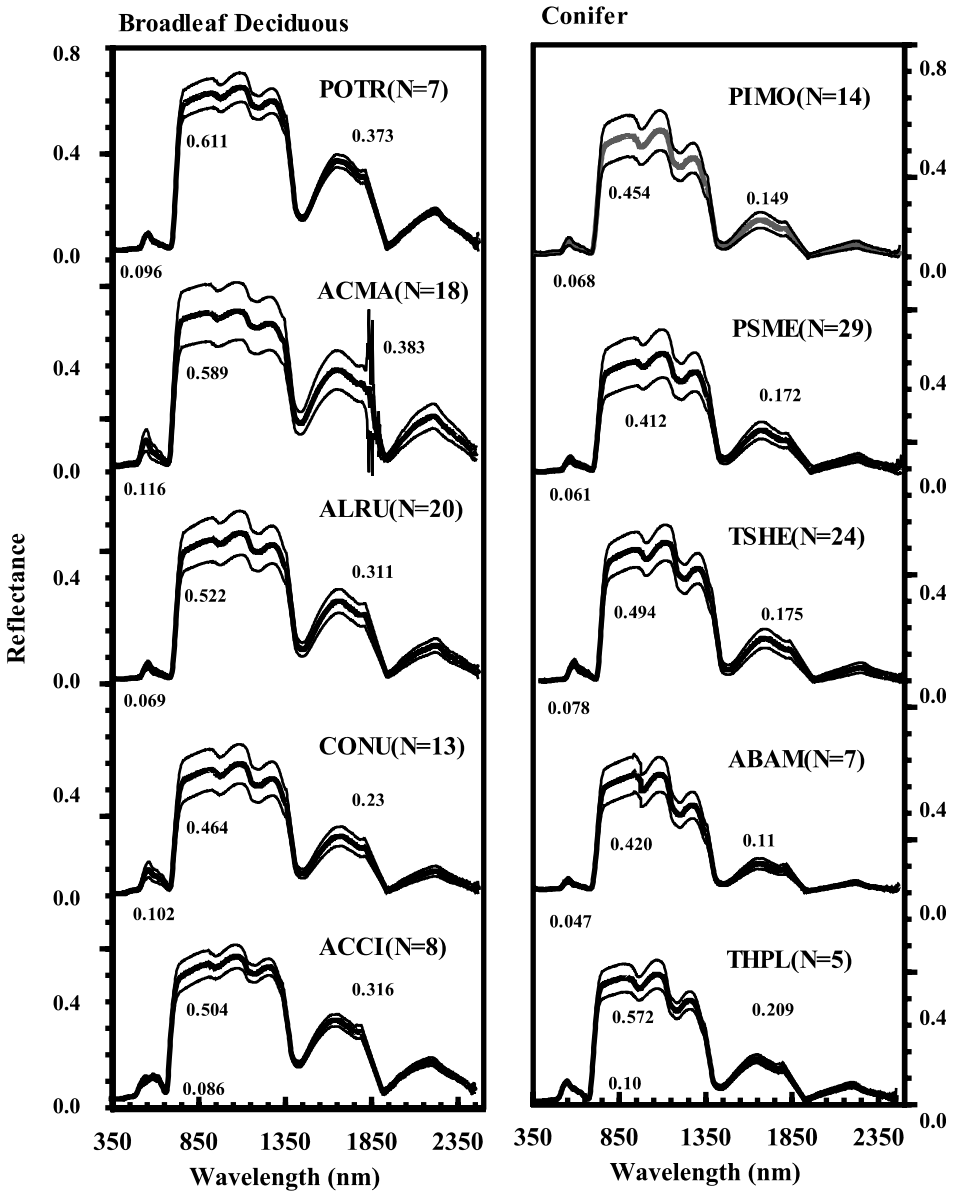

Figure 3. Branch-scale reflectance spectra of five broadleaf deciduous species and five conifer species. Plots show the mean ± SD. The number of spectra used in the average is shown in parentheses. Numbers shown beside each plot correspond to reflectance at 550, 830, and 1,650 nm (in the green, near-infrared (NIR), and short-wave infrared (SWIR) spectral regions, respectively). POTR, *Populus trichocarpa*; ACMA, *Acer macrophyllum*; ALRU, *Alnus rubra*; CONU, *Cornus nuttallii*; ACCI, *Acer circinatum*; PIMO, *Pinus monticola*; PSME, *Pseudotsuga menziesii*; TSHE, *Tsuga heterophylla*; ABAM, *Abies amabalis*; THPL, *Thuja plicata*.

Independent of species, spectral contrast between regions of strong absorption and strong scattering was enhanced at the branch scale (Figure 3). This is evident by comparing the depth of the chlorophyll band at 680 nm to the peak of NIR reflectance around 830 nm. A more subtle increase in contrast is evident when comparing reflectance within a strong water-absorbing band, such as 1,200 nm, to reflectance within an adjacent spectral region. Within broadleaf species and in comparison to leaf-scale spectra, branch-scale spectra had lower visible reflectance, higher NIR reflectance, and enhanced spectral contrast between NIR and SWIR. Within conifers, branch-scale reflectance was less than leaf reflectance at all wavelengths except in THPL, which behaved more like a broadleaf species, perhaps because the orientation of branches minimized shadowing. The contrast between NIR and SWIR, a diagnostic feature separating conifers and broadleaf plants at the leaf scale, became even more pronounced at the branch scale.

Lichen, moss, and bark reflectance. Spectra of lichens, cyanolichens, and mosses show a number of similarities, including very low ultraviolet reflectance, high visible reflectance, prominent chlorophyll absorptions, and strong ligno-cellulose bands in the SWIR (Figure 4). In all four cases, the epiphyte species are spectrally distinct, primarily in the visible, with a wide range of maximum reflectances from low reflectance (around 30%) in PLGL to

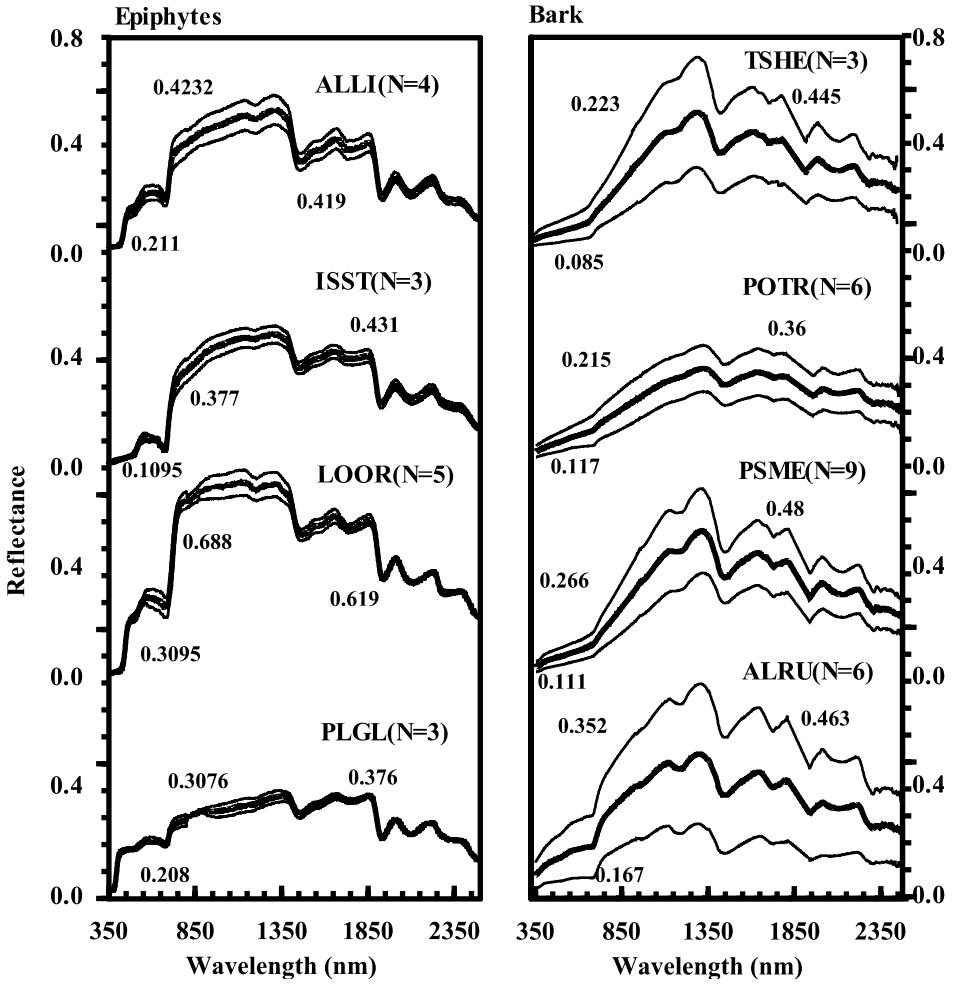

Figure 4. Branch-scale reflectance spectra of four nonvascular epiphytes and four types of nonphotosynthetic vegetation (NPV). Plots show the mean ± SD (above and below the mean). The number of spectra used in the average is shown in parentheses. Epiphyte spectra include an assemblage of Alectoroid lichens (ALLI), *Isothecium stoloniferum* (ISST), *Lobaria oregana* (LOOR), and *Platismatia glauca* (PLGL). Bark spectra include *Tsuga heterophylla* (TSHE), *Populus trichocarpa* (POTR), *Pseudotsuga heterophylla* (PSME), and *Alnus rubra* (ALRU). Numbers shown beside each plot correspond to reflectance at 550, 830, and 1,650 nm (green, near-infrared (NIR), and short-wave infrared (SWIR) spectral regions, respectively).

nearly 70% in LOOR. Spectral features similar to green leaves (that is, chlorophyll absorptions) and nonphotosynthetic vegetation (that is, absorption by ligno-cellulose bands) suggest that nonvascular epiphytes could be confused as a mixture of green leaves and branches.

Bark spectra are shown for two broadleaf and two conifer species (Figure 4). Within-species variance was generally high, but conifer bark was distinct from broadleaf bark by the concave versus convex, respectively, spectral shape between visible and NIR wavelengths. High spectral variability in bark, a major component of NPV, suggests that a single NPV endmember is unlikely to capture the variation within canopies and clear-cuts and indicates that different spectra should be used for each of these land-cover types.

The most spectrally variable material observed at the branch scale was bark, especially ALRU (compare the spectra in Figures 3 and 4). Bark spectra are particularly problematic because of the interplay between the presence of structural material (lignin, structural carbohydrates, and so on) and moisture. Structural components can only be detected when tissue water content is low. When water is present, as in the fresh leaf spectra, water dominates absorption, masking the weaker absorptions seen when the material is dry (Elvidge 1990).

Stand scale reflectance. Because of the large area covered by any AVIRIS pixel (400 m^2), we simplified the analysis by restricting our consideration to only "single" species stands. As a result, our species-level comparison was restricted to several age classes of PSME, two stands of TSHE (Figure 5) and two stands of ALRU (not shown). This comparison is complicated as even planted PSME stands contain other species. For all comparisons, there was at least 80% dominance by the principal species. Recently regenerated clear-cuts (that is, stands less than 10 years old) and ALRU had the highest spectral reflectance (Figure 5a), with NIR reflectance about 39%, green reflectance near 5%, and SWIR reflectance near 20%. Although recently regenerated clear-cuts consisted of a large diversity of plant spe-

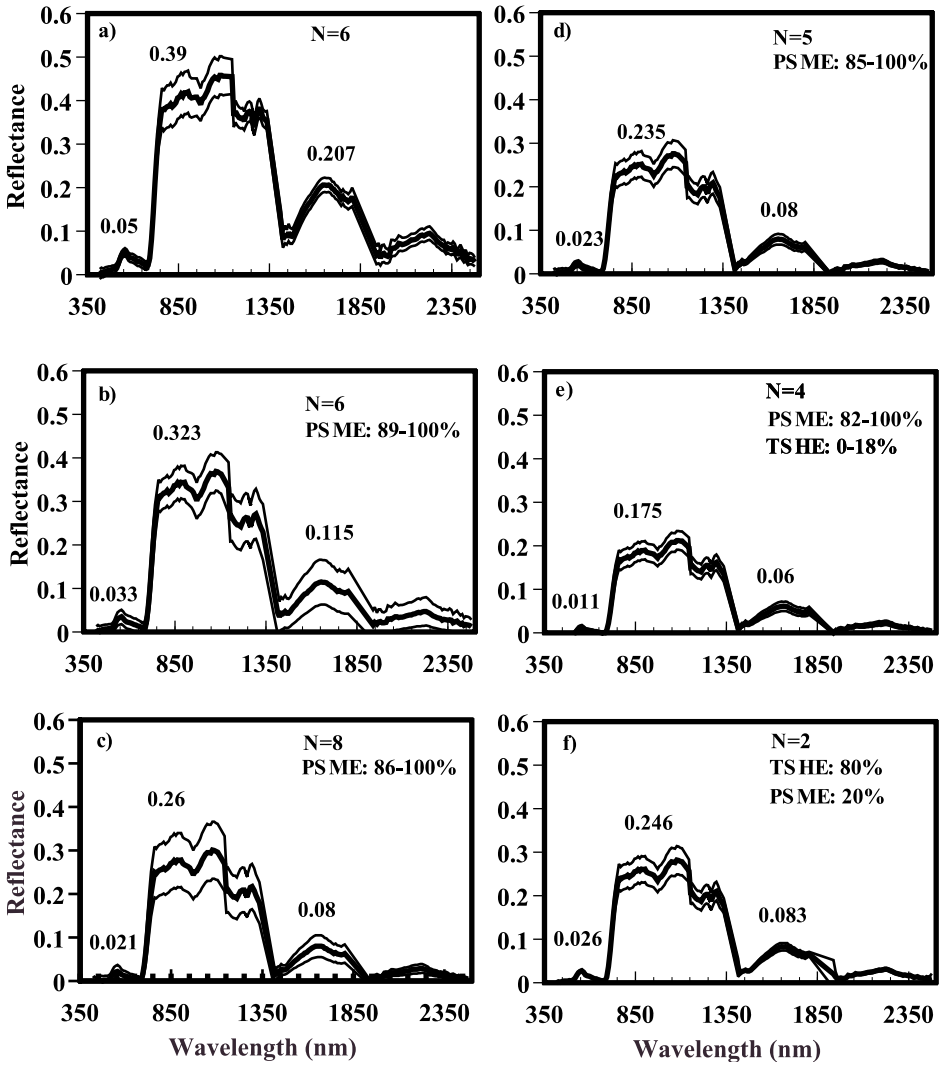

Figure 5. Stand-scale reflectance spectra of a very recently regenerated clearcut (a), four age classes of *Pseudotsuga menziesii* (PSME) (b–e), and an 80-year-old *Tsuga heterophylla* (TSHE) stand (f). Plots show the mean ± SD (above and below the mean). The number of spectra used in the average is shown.

cies and the ALRU stands were dominated by a single species, the two sets of spectra were remarkably similar (not shown). In comparison to branch-scale spectra, stand reflectance decreased at all wavelengths. Whereas leaf-level spectra are dominated by reflectance from a single material, branch-level spectra represent a mixture of materials with highly variable reflectances in which absorption dominates in the visible and scattering in the NIR and SWIR. This differential is further enhanced at the stand level.

The relatively low reflectance observed in recently regenerated clear-cuts was even more pronounced in older conifer stands originating from both clear-cuts and natural disturbances (Figure 5b–e). In these stands, visible light reflectance was lower than branch-scale reflectance by as much as a factor of six. NIR reflectance was also considerably lower, although still as high as 32% for the youngest stands of PSME (Figure 5b). SWIR reflectance showed a decrease intermediate between the visible and NIR parts of the spectrum. A comparison between PSME and TSHE stands within similar age classes (Figure 5d and f) showed few differences between these two species. In contrast, a comparison of PSME between different age classes showed marked differences, producing a general trend of decreasing reflectance with an increase in stand age (Figure 5b–e). Decreased reflectance with increasing stand age most likely reflects changes in canopy structure (Franklin and others 2002).

Statistical comparisons were also performed at the stand scale, using a two sample *t*-test to determine if spectral differences were significant between stands. Following a method of analysis similar to that used at the branch scale, the mean and variance for all stands within an age or species class were used to calculate a *t*-statistic in a paired com-

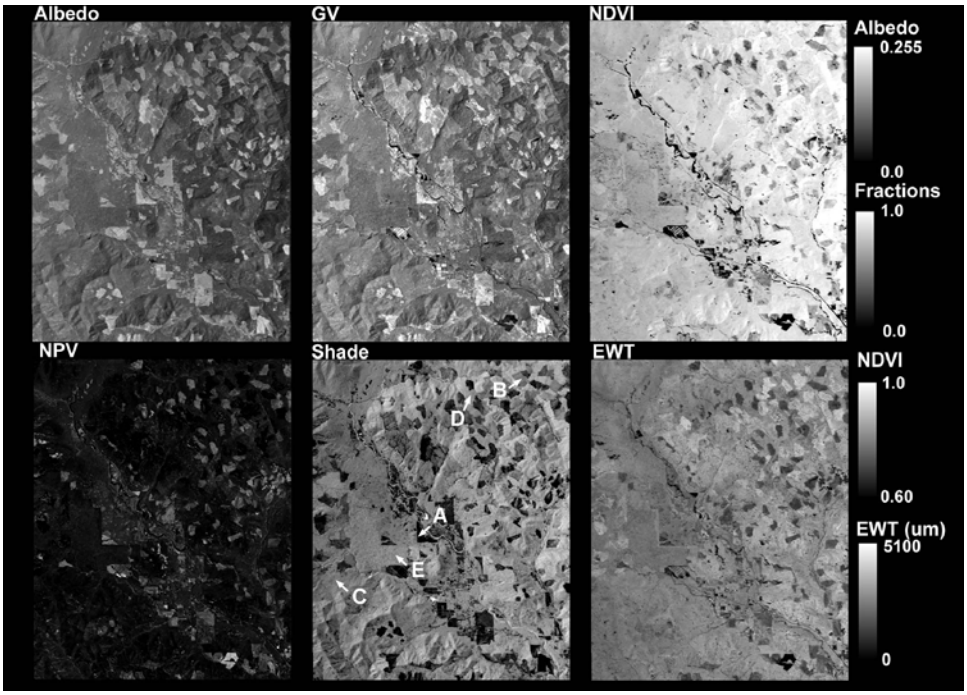

Figure 6. AVIRIS image data from a subset of the study site showing albedo, spectral fractions for non-photosynthetic vegetation (NPV), green vegetation (GV), and shade. The normalized difference vegetation index (NDVI), scaled between 0.6 and 1.0, and equivalent water thickness (EWT), scaled between 0 and 5,100, are shown to the right of spectral fractions. Five locations that represent a diversity of age classes are in the shade image. These stands are **A**) 8, **B**) 29, **C**) 70, **D**) 132, and **E**) 461 years old.

parison. Six classes were compared, including recently regenerated clear-cuts (6–10 years old), young stands (11–30 years old), two intermediate age classes of PSME (31–50 and 51–100 years old), an old stand of PSME (101–200 years old), and two stands of TSHE listed as 80 years old by the USFS. As would be expected based on their spectra (Figure 5), recently regenerated clear-cuts were significantly different from all conifer classes (78%–100% of AVIRIS wavelengths at $\alpha = 0.05$). When we compared the 80-year-old TSHE stands to the 46–100-year-old stands of PSME, only 2.6% of the wavelengths proved to be significantly different at $\alpha = 0.05$. In contrast, age-related differences proved to be more significant. When we compared one age class to the next oldest age classes, the percentage of wavelengths that were significant varied from 13.7% (11–30 compared to 31–50 years old) to a high of 48.4% between the 51–100- and 100–200-year-old age classes. The only two contiguous age classes that proved to be spectrally inseparable were the 31–50 and 51–100-year-old classes, primarily due to large spectral variance and small sample sizes.

Stand Scale: Structural Attributes

Albedo, spectral fractions (GV, NPV, shade), NDVI, and EWT were calculated from AVIRIS data as previously described and mapped to examine how these measures varied across structurally distinct land-cover types (Figure 6). Five distinct locations are marked as A to E on the shade panel of this figure; these locations range from a newly regenerated clear-cut (point A, 8 years old) to a 461-year-old PSME/TSHE forest (that is, the entire T. T. Munger Natural Area in which the canopy crane is situated, shown as E). Very young stands (that is, less than 10 years old) have the highest albedo (also broadleaf stands, not indicated), lowest EWT, and highest GV and NPV (Figure 6, point A). In the shade and albedo images, these stands appear as black and light irregular patches, respectively. Subsets of these stands do not have a very high GV, but they have a high NPV fraction, presumably due to differences in site preparation (for example, retaining slash on site). NDVI and EWT peak in relatively young stands (point B: 29-year-old stand in Figure 6). These stands also have the lowest NPV and moderate albedo. It is easiest to see these stands in the EWT panel (Figure 6), where they appear the brightest. In other images (that is, panels), they are more difficult to distinguish from older age classes. As shown in Figure 6, after this relatively young stand peaks in NDVI and EWT, stands tend to show a decrease in EWT, an increase in shade, and an increase in NPV (points C to E); however, most of these patterns are fairly subtle, resulting in intermediate grays in all of the images except NPV.

Exposed soil cover was generally low throughout the study area; the highest fractions occurred along gravel bars and roads and in open fields (not shown). NPV was also low, with low values in

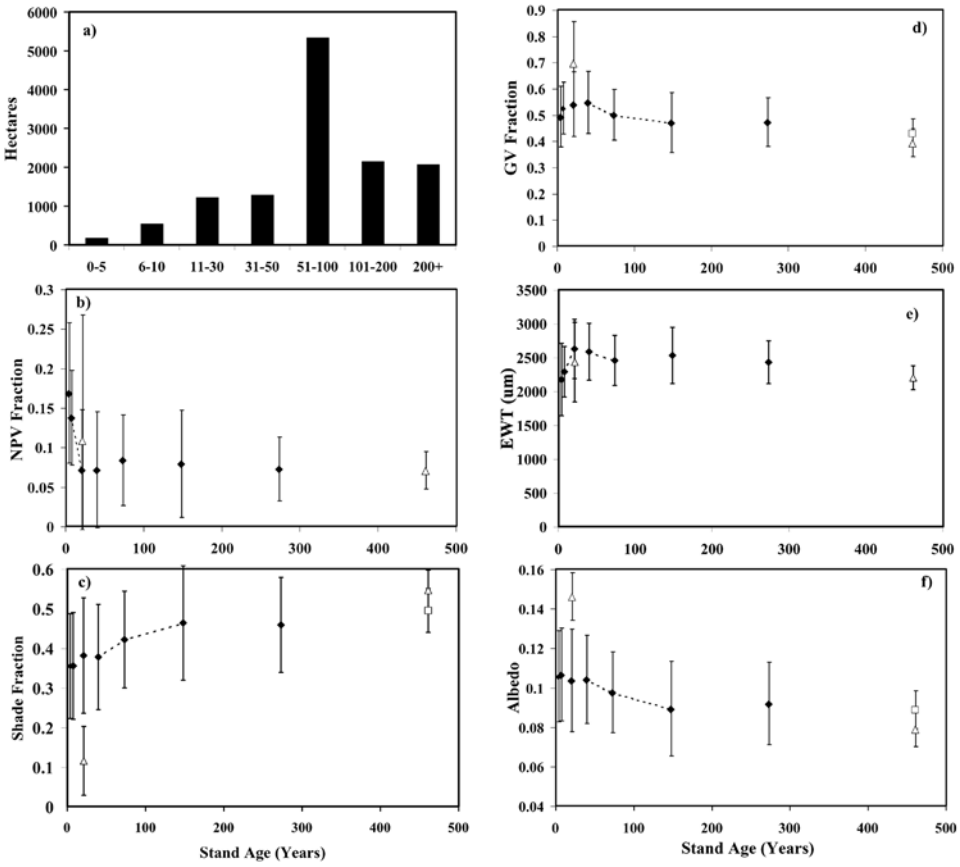

Figure 7. AVIRIS structural measures for various age classes. **a** Number of hectares in each class. Panels **b, c, d, e,** and **f** show the nonphotosynthetic vegetation (NPV), shade, and green vegetation (GV) fractions, equivalent water thickness (EWT), and albedo, respectively. Values for the 21-year-old stand and the Wind River Canopy Crane Research Facility (WRCCRF) are shown as open triangles. Median age of an age class is plotted along the x-axis. Statistically significant differences between age classes ($\alpha = 0.01$) are shown as dashed lines connecting two points. Albedo and shade are also plotted for the T. T. Munger area as open squares. Values were extracted from a subset of the full AVIRIS flightline (upper left, 45°55'55″N, 121°59'54″W; lower right, 45°46'52″N, 121°53'6″W, North American Datum, 1927).

forests between 50 and 500 years old and the highest fractions in recently regenerated clear-cuts and stands younger than 20 years.

The greatest range in values was observed in the GV and shade fractions. Shade includes both topographic illumination and textural variation due to tree size and tree and stand architectural features. The highest GV occurred in newly regenerated clear-cuts and riparian areas. Second-growth forests showed higher GV than old-growth forests. Shade was inversely related to GV and albedo. Low shade was found in recently regenerated clear-cuts and riparian areas.

In addition to stand attributes (that is, age, composition, and structure), topography and lighting geometry also affects the images shown in Figure 6. Albedo, which varies with stand age, was lowest on northwest-facing slopes and on the eastern edge of the image. Shade, which is the inverse of albedo, was highest on northwest-facing slopes and on the eastern edge. Finally, NDVI was highest when there was a combination of dense vegetation and low albedo. The impact of slope aspect and viewing geometry is illustrated by the strong gradient in brightness in the NDVI panel on Figure 6, where the right side is brighter than the left.

A comparison between remotely sensed structural parameters and stand age illustrates differences among the age classes, some of which were statistically significant (Figure 7). As shown in Figure 7a, this landscape is dominated by second-growth forests, with the largest area in the 51–100-year age class. Older stands (101–200 and more than 200 years old) constitute the next most abundant age classes. Recently regenerated clear-cuts, less than 10 years old, represent a very small area, whereas stands in the 11–30- and 31–50-year age classes comprise similar but also relatively small areas. The WRCCRF is located in one of the largest blocks of forest in the area and accounts for a significant proportion of the old-growth forest in the region (see Figure 1).

Based on spectral fractions, albedo, shade, GV and NPV, the general successional pattern can be characterized as a transition from stands consisting of high NPV, low EWT (that is, lower leaf cover), highest albedo, and lowest shade, to stands with higher shade, higher EWT, and lowest albedo (Figure 7). Statistically significant differences between a few of the age classes were observed in all of these remotely sensed measures of structure (dashed lines). For example, a comparison between the

6–10- and 11–30-year-old classes showed a statistically significant drop in NPV and an increase in EWT (Figure 7b and e). Significant increases in shade and decreases in albedo were also observed when comparing the 31–50-year-old stands to the 51–100-year-old stands and when comparing the 51–100-year-old stands to the next oldest age class. Although patterns can be discerned, high standard deviations around means and a relatively narrow range of means resulted in few significant differences. As with any data set, the pattern and the correspondence between changes, increasing or decreasing, in different remotely sensed spectral fractions represent important interpretative tools. However, an understanding of the factors that affected the observed variation for any age class will be equally important. As this understanding unfolds, an increasing proportion of the variation should be accounted for, and spectral differences between stands should be visually and statistically more apparent.

Values of the spectral fractions and their patterns can be used to address the question of how representative the two flux sites are (Figure 7). As shown, the 21-year-old site had significantly higher albedo, GV, and NPV and significantly lower shade than stands of similar ages based on a *t*-test. In contrast, the old-growth stand at and surrounding the WRCCRF had values of GV, NPV, EWT, shade fraction, and albedo that fit the patterns shown in Figure 7. The albedo value reported here for the WRCCRF (0.079) compares closely to the independently estimated value of 0.075 (Mariscal and others 2004). Because the site is situated in the eastern and elevationally lowest part of the T. T. Munger Natural Area, the approximate 4-ha area around the crane was analyzed separately from the more westerly parts of the Natural Area. When comparing the WRCCRF to the surrounding T. T. Munger area, most measures were similar, although the WRCCRF is located in one of the darkest sections of the forest and has an albedo 1% lower than the average albedo of 0.089 and a shade value higher than the T. T. Munger area (that is, 54.5% and 49.5%, respectively) (Figure 7).

Relationship to Leaf Area Index

A total of 39 sites—35 vegetated and four nonvegetated—were used for the two comparisons (EWT and NDVI estimated LAI, respectively, versus measured LA) (Figure 8), and the following nonlinear regressions models were found:

$$EWT_{site} = (2364.0 - 2364.0e^{-0.2433*LAI_{total}}) + 141.4 \quad (4)$$

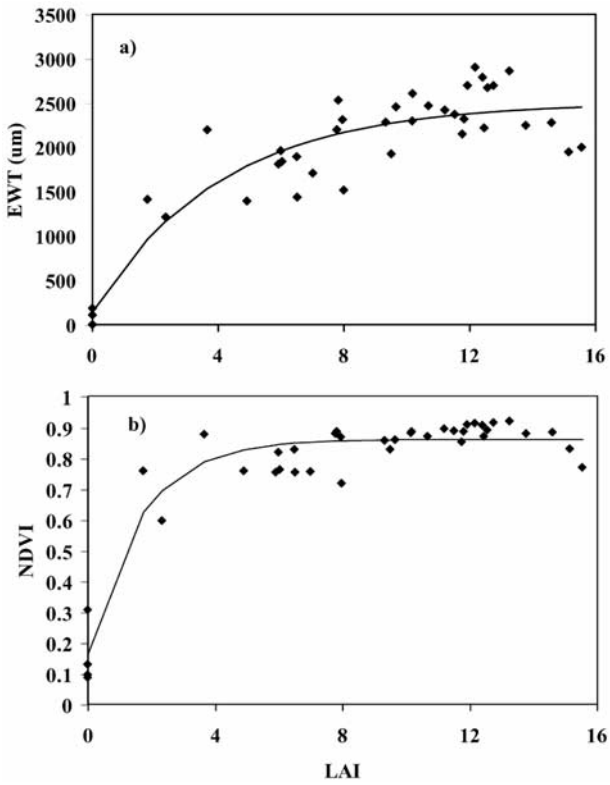

Figure 8. Relationship among leaf area index (LAI), equivalent water thickness (EWT), and normalized difference vegetation index (NDVI). **a** Plot of LAI versus EWT and the best-fit exponential decay model. **b** Plot of LAI versus NDVI.

$$NDVI_{site} = (0.6979 - 0.6979e^{-0.6162*LAI_{total}}) + 0.1635 \quad (5)$$

An *F*-test yielded a significant *P* value of less than 0.0001 for both regression models. At 95% of the maximum measured value (that is, 0.95*b*), the LAI estimated by the EWT relationship was 9.08 and the LAI estimated by NDVI was 5.17. Of the 35 vegetated sites, all but four had LAI in excess of the 95% maximum for NDVI. Fourteen forested sites were below the 95% maximum for EWT. The WRCCRF is at the upper end of the 95% maximum for EWT.

Discussion

Spectral features change with the scale of the measurement. At each larger scale, new features are included in the measurements that were either absent or of minor importance at lower scales. At the leaf scale, leaf biochemical variation—specifically in pigments, water, and structural carbohydrates—

were of key importance in differentiating species (Figure 2). Additionally, anatomical differences such as cell size, air spaces, and cell wall thickness contribute to species differences, particularly at NIR and SWIR wavelengths (Gausman 1985). As the spatial scale increases to the branch, other plant materials, including wood and epiphytes, are incorporated into the measurement. At this scale, the differential impact of light absorption in the visible and light scattering in the NIR becomes more important. At the stand or landscape scale, a complex array of features, including some technical ones (that is, illumination and viewing geometry), affect the images derived and therefore their interpretation. To simplify, one could say that any image is a complex mixture of different absorptive, reflective, and light-scattering surfaces—at this level, then, GV and NPV dominate. It is also important to note that the types of GV (deciduous broadleaf versus coniferous needle-leaf) and especially NPV (that is, bark, wood) are critical. As stands become structurally more complex and trees become taller, shading and the scattering of light further complicate and affect the image. The typical progression of forested stands in the Pacific Northwest can then be interpreted by the interplay of these spectral elements and both their absolute and relative values. Most of the landscape shown in both Figures 1 and 6 was shaped by 100-plus years of timber harvesting, settlement, and fires. There was a period from 1902 until 1929 during which at least 19 wildfires, covering between 405 and 107,004 ha, burned and reburned much of the area (J.F. Franklin personal communication). There is also evidence of severe fires in 1845 and 1875. Following such major disturbances, vertical and horizontal structure may be simple (typical clear-cut or site burned multiple times) or complex (typical fire), depending on whether the dead trees and snags have been removed, hidden by developing canopies, or decomposed. Recovery of green vegetation and the development of forest structure is similarly complex, depending on whether there was site preparation and subsequent planting (clear-cut) or natural regeneration (fire). As stands—particularly those that are managed—develop, there is a period of increases in green foliage (GV, NDVI, and EWT increase) and decreases in NPV and albedo. At the same time, shading increases. In a few cases, shading and NPV can dominate young stands when, for example, diseases such as Phellinus root rot open up the stand (for example, the 21-year-old study site). More typically, gaps and openings do not occur until stands become older than 100–200 years.

Broad spectral patterns observed at leaf scales translate to predictable patterns at branch scales. Multiple NIR light scattering enhances the expression of strong absorption features in canopies (Heilman and others 1996; Asner 1998). As a result, leaf-scale differences in transmittance propagate into canopy reflectance, enhancing spectral separability between species. As expected, scattering had less impact on conifers than on broadleaf plants due to lower transmittance and higher absorptance by needles.

Many of the species sampled here have not been previously described spectrally. Species-level differences were most significant at the branch scale—a new finding. At this scale, all of the species were significantly different over at least a portion of the spectrum. In contrast, species were least distinct at stand scales. Although only a few species could be compared, few significant differences were observed when we compared PSME and TSHE stands of a similar age. In a similar fashion, stands dominated by a single broadleaf species, ALRU, were significantly different from mixed-species clear-cuts over only a very few AVIRIS wavelengths. Significant differences were observed when comparing young and old stands of PSME and when comparing broadleaf and coniferous stands. The leaf scale represented an intermediate level of separability between branch and stand scales.

A number of researchers who have compared plant spectra at multiple scales reported similar results. For example, Williams (1991) noted that conifer reflectance decreased dramatically from leaf to canopy scales. He also found, by comparing spectra from conifers to those from sugar maple (*Acer saccharum*), that conifers are more absorptive than this broadleaf tree species. Rock and others (1994) compared needle and branch spectra for red spruce (*Picea rubens*) and eastern hemlock (*Tsuga canadensis*), for 1st- and 2nd-year needles. They also noted spectral differences between these two species, especially in absorptance. However, in contrast to this study, they also compared 1st- and 2nd-year foliage, noting that 2nd-year foliage can be characterized as having lower reflectance than 1st-year foliage, with even greater differences observed at the branch scale. The importance of leaf age, as a factor modifying leaf reflectance, should be considered when interpreting how spectral separability is discussed in this paper, especially when conifer spectra are compared at leaf and branch scales. The effects of leaf aging may either depress or enhance the species-level differences observed in this study.

Poor spectral separation of plant species at the stand scale reflects the confounding effects of illumination, canopy structure, and the spatial resolution of the sensor. Branch-scale analysis suggests

that, given a spatial resolution fine enough to resolve individual crowns, species can be separated. However, for a majority of the plants studied here, the 20-m spatial resolution of AVIRIS was insufficient to guarantee that only one species was imaged. This is particularly true of newly regenerated clear-cuts or very young, mixed stands, where many plant species occur within a 20 × 20 m pixel. Very large trees should be distinct at the individual pixel scale, provided that individual crowns can be identified on the image and in the field. However, at the scale of analysis used here, species-specific spectral differences were obscured by canopy structure. At this scale, age-related differences become significant. Broadleaf and coniferous plants are readily distinguished at all spatial scales.

Several of the remotely sensed structural measures used in this study appear to be promising for showing patterns of conifer succession. Young clear-cuts typically are heterogeneous, with variable canopy cover, exposed soil, and slash. As the stand ages, canopy closure occurs, which should decrease NPV and increase GV and EWT (LAI). During the stem exclusion phase, a uniform, even-aged stand is expected to produce some of the highest GV and EWT (LAI) measurements. This is what was observed for the 11–30- and 31–50-year age classes. As a stand continues to age and gaps form, it typically becomes increasingly heterogeneous, species composition shifts, and the amount of standing dead material increases. Higher shade fractions, higher NPV, and lower albedo are expected to occur in older forests. Higher NPV fractions were observed when we compared all stands older than 51 years to the 11–30- and 31–50-year-old classes, but the differences were not significant. We observed the most significant changes in shade and albedo in the 51–100- and 101–200-year-old age classes. A lack of statistically significant differences between the 101–200-year-old and 200+ age classes suggests that stand-averaged, remotely sensed structural measures are no longer sensitive to age differences between these two classes at this site. Similar observations for this region were reported by Sabol and others (2002), who show a clear successional pathway for stands up to 64 years old, but could not distinguish older stands.

Standard successional models might be expected to produce many of the temporal patterns we observed, and thus our results could be considered confirmation of existing theory (for example, Franklin and others 2002). However, one of the greatest strengths of remote sensing is the fact that it provides a spatial representation of patterns and multiple measures of stands of similar age. Although the mean temporal trends in shade, albedo, EWT, and (to a lesser extent) GV follow trends we might anticipate from succession, sources of variance in these variables highlight a potential strength of remote sensing. A good example is provided by the 21-year-old stand. Based on an age map and standard models of forest succession, we would predict one pattern, yet our results show that the 21-year-old stand is anomalous with respect to similar age classes. Although the large error bars for a specific age class decreased statistical significance when comparing age classes, they highlight sources of variance that represent information regarding spatial variability in stands of similar ages. Likely sources of variance include site quality, site treatment (that is, thinning), disease or insect attack, or biological legacy such as the type and scale of disturbance (Oliver and Larson 1990). Furthermore, the kind of high-quality stand information that is routinely available from the USFS is lacking for many other areas of the Earth. In this case, remote sensing may provide the best data available for analyzing forest structure.

Canopy reflectance and EWT represent two of the most potentially useful measures examined in this study. Reflectance can be used to estimate albedo, a variable needed to determine net radiation. The high albedo of the 21-year-old stand, which was nearly double that of the WRCCRF, may help to account for the lower net radiation and lower evapotranspiration observed in this stand when compared to the WRCCRF in 1999 (Chen and others 2004). EWT shows promise for improving estimates of LAI, which is necessary for scaling models to estimate regional fluxes (for example, see Running 1994). When EWT and NDVI were compared to the LAI measured at 35 vegetated sites, both measures showed exponential decay in which the rate of increase decreased with increasing LAI. However, NDVI reached 95% of the maximum in the model at an LAI of 5.17. As a result, 89% of the 35 vegetated sites had an LAI greater than the maximum LAI that could be estimated using NDVI. Furthermore, NDVI proved to be highly sensitive to aspect and lighting, with the highest values found on northwest-facing slopes and on the eastern edge of the scene (NDVI panel, Figure 6). EWT, in contrast, reached 95% of the maximum in the model at an LAI of 9.08, reducing the number of sampled stands that were above this maximum to 60% (21 of 35). As a result, EWT could be used to estimate LAI over a greater range of sites than NDVI, including many of the stands within the study region and the WRCCRF. The potential use of EWT as an alternate measure of LAI for model inputs should be explored further. However, alternate approaches

that relate LAI to EWT should also be considered. The relatively low LAI asymptote reached by the EWT extinction-based model is still lower than more than half of the vegetated sites sampled in this study and lower than published values for other parts of the Pacific Northwest (for example, see Spanner and others 1994). Furthermore, leaf-scale differences in the expression of liquid water observed between conifers and broadleaf species leave open questions about whether one relationship is appropriate across major taxonomic groups.

We have several recommendations to make regarding the potential of remote sensing and its relevance to the broader goals of understanding ecosystem responses to climate change. First, the two flux towers located within the flight line represent only a small portion of the continuum of age classes within the area. The region is highly heterogeneous, with the most abundant class within the 51–100-year-old category. Although both the old-growth and the 21-year-old sites represent important endmembers to the range of stands found in this area, the most abundant regional age class is missing. The importance of this age class is further supported by remotely sensed estimates of EWT, albedo, and shade, which showed that the 51–100-year-old class represents a seral stage in which significant changes in canopy structure are occurring (Franklin and others 2002). In the event that new tower sites are established, remote sensing should play a key role in siting them strategically. Furthermore, the sites could be selected to minimize within-stand variance, which was evident in the 21-year-old site as reported here.

AVIRIS data have been acquired over a wide range of ecosystems across North America, including many that have operational flux towers (for example, Harvard Forest and Howland, Maine). A number of the remotely sensed structural measures described here, such as albedo, EWT, and spectral fractions, can readily be determined for other sites to aid in scaling efforts. At the leaf and branch scales, it is clear that different species can be separated, with the best separation occurring at the branch scale. At the landscape scale, AVIRIS offers tradeoffs. The 20×20 m pixel size is potentially too coarse for species discrimination; however, AVIRIS produces image information over areas of 500 km^2 or more in size and in 224 different wavelengths, thereby providing spatial, as well as spectral, context to aid interpretation.

ACKNOWLEDGMENTS

We thank Dr. Jeff Dozier for the loan of an ASD spectrometer for the 1999 field campaign, Edward Collins for Modtran simulations used for albedo calculations, Dr. David Shaw for collecting the nonvascular epiphytes from the WRCCRF, and George J. Scheer for measuring the epiphyte spectra. AVIRIS data used in this study were supplied by the NASA Jet Propulsion Laboratory, which also supplied an ASD field spectrometer in 1996. Access to the WRCCRF was kindly supplied by the USDA Forest Service Pacific Northwest station, which also facilitated research in the area. Funding for this research was supported by the Office of Science (BER), US Department of Energy, through the Western Regional Center of the National Institute for Global Environmental Change under cooperative agreement no. DE-FC03-90ER61010. Finally, we thank two independent reviewers and Dr. Steven Seagle for helpful comments on the manuscript. Any opinions, findings, and conclusions or recommendations expressed herein are those of the authors and do not necessarily reflect the view of the DOE.

REFERENCES

Adams JB, Smith MO, Gillespie AR. 1993. Imaging spectrometry: interpretation based on spectral mixture analysis In: Pieters CM, Englert PRemote geochemical analysis: elemental and mineralogical composition; vol 7 New York: Cambridge University Press. p p 145–166.

Asner GP. 1998. Biophysical and biochemical sources of variability in canopy reflectance. Remote Sens Environ 64:234–53.

Berk A, Bernstein LS, Robertson DC. 1989, MODTRAN: a moderate resolution model for LOWTRAN 7. Final Report GL-TR-0122. Hanscom AFB, MA.: AFGL, pp 42 p.

Chen J, Paw U KT, Ustin SL, Suchanek TH, Falk M, Brosofske KD, Wang X, and others. 2004. Net ecosystem exchanges of carbon, water, and energy in young and old-growth Douglas-fir forests. Ecosystems 7:534–44.

Cohen WB, Spies TA. 1992. Estimating structural attributes of Douglas-fir/western hemlock forest stands from Landsat and SPOT imagery. Remote Sens Environ 41:1–17.

Cohen WB, Spies TA, Bradshaw GA. 1990. Semivariograms of digital imagery for analysis of conifer canopy structure. Remote Sens Environ 34:167–78.

Cohen WB, Spies TA, Swanson FJ, Wallin DO. 1995. Land cover on the western slopes of the central Oregon Cascade range. Int J Remote Sens 20(3):421–35.

Elvidge CD. 1990. Visible and near-infrared reflectance characteristics of dry plant materials. Int J Remote Sens 11(10):1775–95.

Franklin JF, Spies TA, Van Pelt R, Carey AB, Thornburgh DA, Berg DR, Lindenmayer DB, and others. 2002. Disturbances and structural development of natural forest ecosystems with silvicultural implications, using Douglas-fir forests as an example. For Ecol Manage 155(N1–3)SI:399–423.

Frazer GW, Trofymow JA, Lertzman KP. 2000. Canopy openness and leaf area in chronosequences of coastal temperate rainforests. Can J For Res 30(2):239–56.

Gamon JA, Field CB, Goulden ML, Griffin KL, Hartley AE, Geeske J, Penuelas J, and others. 1994. Relationship between NDVI, canopy structure, and photosynthesis in three California vegetation types. Ecol Appl 5(1):28–41.

Gates DM, Keegan HJ, Schleter JC, Weidner VR. 1965. Spectral properties of plants. Appl Optics 4(1):11–20.

Gausman HW. 1985, Plant leaf optical properties in visible and near-infrared light. Graduate Studies Texas Tech University No. 29. Lubbock (TX): Texas Tech Press, pp 78.

Gong P, Pu RL, Miller JR. 1995. Coniferous forest leaf area index estimation along the Oregon Transect using compact airborne spectrographic imager data. Photogram Eng Remote Sens 61(9):1107–17.

Goward SN, Huemmrich KF, Waring RH. 1994. Visible-near-infrared spectral reflectance of landscape components in western Oregon. Remote Sens Environ 47(2):190–203.

Green RO, Conel JE, Margolis JS, Bruegge CJ, Hoover GL. 1991. An inversion algorithm for retrieval of atmospheric and leaf water absorption from AVIRIS radiance with compensation for atmospheric scattering In: Green ROProceedings of the 3rd Airborne Visible/Infrared Imaging Spectrometer (AVIRIS) Workshop. 20–21 May Pasadena, CA, USA: Jet Propulsion Laboratory. p p 51–61.

Green RO, Conel JE, Roberts DA. 1993. Estimation of aerosol optical depth and calculation of apparent surface reflectance from radiance measured by the airborne visible-infrared imaging spectrometer (AVIRIS) using MODTRAN2. SPIE Conference 1937: Imaging Spectrometry of the Terrestrial Environment, Greg Vane, Orlando, FL, 14–15 April 1993; The International society for Optical Engineering (SPIE), Bellingham, WA, p 2–5.

Green RO, Eastwood ML, Sarture CM, Chrien TG, Aronsson M, Chippendale BJ, Faust JA, and others. 1998. Imaging spectroscopy and the airborne visible infrared imaging spectrometer (AVIRIS). Remote Sens Environ 65(3):227–48.

Heilman PE, Hinckley TM, Roberts DA, Ceulemans R. 1996. Production physiology In: Stettler RF, Bradshaw HW, Heilman PE, Hinckley TMBiology of Populus and its implications for management and conservation Washington (DC): NRC Research Press. p 459–490.

Johnson LF, Hlavka CA, Peterson DL. 1994. Multivariate analysis of AVIRIS data for canopy biochemical estimation along the Oregon Transect. Remote Sens Environ 47:216–30.

Law BE, Waring RH. 1994a. Remote sensing of leaf area index and radiation intercepted by understory vegetation. Ecol Appl 4:272–9.

Law BE, Waring RH. 1994b. Combining remote sensing and climatic data to estimate net primary production across Oregon. Ecol Appl 4:717–28.

Lefsky MA, Cohen WB, Acker SA, Parker GC, Spies TA, Harding D. 1999. Lidar remote sensing of the canopy structure and biophysical properties of Douglas-fir western hemlock forests. Remote Sens Environ 70(3):339–61.

Mariscal MJ, Martens SN, Ustin SL, Chen J, Weiss SB, Roberts DA. 2004. Light transmission profiles in an old-growth forest canopy: Simulations of photosynthetically active radiation using spatially explicit radiative transfer models. Ecosystems 7:454–67.

Means JE, Acker SA, Harding DA, Blair JB. 1999. Use of large-footprint scanning airborne lidar to estimate forest stand characteristics in the western cascades of Oregon. Remote Sens Environ 67:298–308.

Oliver CD, Larson BC. 1990, Forest stand dynamics. New York: McGraw-Hill, pp 467.

Peterson DL, Waring RH. 1994. Overview of the Oregon Transect ecosystem research project. Ecol Appl 4(2):211–25.

Peterson DL, Spanner MA, Running SW, Teuber KB. 1987. Relationship of thematic mapper simulator data to leaf area index of temperate coniferous forests. Remote Sen Environ 22:323–4.

Potter CS, Randerson JT, Field CB, Matson PM, Vitousek PM, Mooney HA, Klooster SA. 1993. Terrestrial ecosystem production: a process model based on global satellite and surface data. Global Biogeochem Cycles 7:811–41.

Roberts DA, Green RO, Adams JB. 1997. Temporal and spatial patterns in vegetation and atmospheric properties from AVIRIS. Remote Sens Environ 62:223–40.

Roberts DA, Brown KJ, Green R, Ustin S, Hinckley T. 1998a. Investigating the relationship between liquid water and leaf area in clonal Populus. In: Green RO, editor. Proceedings of the 7th AVIRIS Earth Science Workshop. Jet Populsion Laboratory 12–16 Jan 1998, Pasadena, CA, USA. p 335–344.

Roberts DA, Batista G, Pereira J, Waller E, Nelson B. 1998b. Change identification using multitemporal spectral mixture analysis: applications in eastern Amazonia In: Elvidge C, Lunetta RRemote sensing change detection: environmental monitoring applications and methods Ann Arbor (MI): Ann Arbor Press. p p 137–61.

Rock BN, Williams DL, Moss DM, Lauten GN, Kim M. 1994. High-spectral resolution field and laboratory optical reflectance measurements of red spruce and eastern hemlock needles. Remote Sens Environ 47:176–89.

Running SW. 1994. Testing forest-BGC ecosystem process simulations across a climatic gradient in Oregon. Ecol Appl 4(2): 238–47.

Sabol DE, Gillespie AR, Adams JB, Smith MO, Tucker CJ. 2002. Structural stage in Pacific Northwest forests estimated using simple mixing models of multispectral images. Remote Sens Environ 80(1):1–16.

Sellers PJ. 1985. Canopy reflectance, photosynthesis and transpiration. Int J Remote Sens 6:1335–72.

Sellers PJ, Randall DA, Collatz CJ, Berry JA, Field CB, Dazlich DA, Zhang C, and others. 1996. A revised land surface parameterization (SiB2) for atmospheric GCMs. Part 1. Model formulation. J Clim 9:676–705.

Shaw DC, Franklin JF, Bible K, Klopatek J, Freeman E, Greene S, Parker GG. 2004. Ecological setting of the Wind River old-growth forests. Ecosystems 7:427–39.

Smith MO, Ustin SL, Adams JB, Gillespie AR. 1990. Vegetation in deserts. I. A regional measure of abundances from multispectral images. Remote Sens Environ 29:1–26.

Spanner MA, Johnson L, Miller J, McCreight R, Freemantle J, Runyon J, Gong P. 1994. Remote sensing of seasonal leaf area index across the Oregon Transect. Ecol Appl 4(2):258–71.

Suchanek TH, Mooney HA, Franklin JF, Guckinski H, Ustin SL. 2004. Carbon dynamics of an old-growth forest. Ecosystems 7:421–26.

Thomas SC, Winner WE. 2000. A rotated ellipsoidal angle density function improves estimation of foliage inclination distributions in forest canopies. Agric For Meteorol 100:19–24.

Tucker CJ. 1979. Red and photographic infrared linear combinations for monitoring vegetation. Remote Sens Environ 8:127–50.

Williams DL. 1991. A comparison of spectral reflectance properties at the needle, branch and canopy level for selected conifer species. Remote Sens Environ 35:79–93.

Woolley JT. 1971. Reflectance and transmittance of light by leaves. Plant Physiol 47:656–62.